# ASSESSMENT OF RAINFALL INFLUENCE ON SENTINEL-1 TIME SERIES ON AMAZONIAN TROPICAL FORESTS AIMING DEFORESTATION DETECTION IMPROVEMENT

J. Doblas[1], A. Carneiro[1], Y. Shimabukuro[1], S. Sant'Anna[1], L. Aragão[1]
[1] INPE, Remote Sensing Division, São José dos Campos, Brazil - (juan.doblas, arian.carneiro, yosio.shimabukuro, sidnei.santanna, luiz.aragao)@inpe.br

**KEY WORDS:** Sentinel-1, Time series, Change Detection, Rainfall Influence, Forests, Amazon.

**ABSTRACT:**

This work aims to determinate the relationship between C-band SAR backscattering measurements over Amazonian tropical forests and hourly precipitation rates, and to study the feasibility of a SAR-anomaly masking method based on orbital rain measurements. To do so, a comprehensive dataset of ESA's Sentinel-1 backscattering data and the concomitant GPM-IMERG precipitation data was collected and analysed. Backscattering anomalies were characterized in a statistically meaningful way. GAM models were then adjusted to the backscatter-rain data pairs. The computed models show a positive correlation between non-anomalous backscattering values and accumulated rain, of approximately 0,2 $dB/mm{\cdot}h^{-1}$ and 0,4 $dB/mm{\cdot}h^{-1}$ for VV and VH polarizations. Negative anomalies, which can easily mislead deforestation algorithms, have a strong negative correlation with rain rate observed at the time of the SAR acquisition. This is especially true for VV measurements. The subsequent anomaly masking procedure, based on computed accumulated and hourly rain thresholding, yielded unsatisfactory results. These poor results are probably due to the coarse resolution of the 0.1° GPM-IMERG data, which is insufficient to track anomaly-generating atmospheric events such as storm rain cells. Rain-related changes in SAR backscattering can compromise deforestation detection algorithms, and further research and sensor developing is needed to increase spatial resolution of precipitation measures, to reach an optimal backscattering anomaly screening.

## 1. INTRODUCTION

Early deforestation detection in tropical forests has become a priority for governments and civil society organizations throughout the world. In this context, Early Warning Systems (EWS), which are defined as a collection of algorithms and procedures able to identify tree loss or disturbance, on a periodic (monthly, weekly or even daily) basis (Petersen, Renschler, and Weisse, 2018), become a key aspect of deforestation reduction initiatives. EWS has been a crucial element to reinforce public policies that have led to significative deforestation rates decrease in Brazil (Soares-Filho *et al.*, 2010; Assunção, Gandour, and Rocha, 2013; Nepstad *et al.*, 2014) and Peru (Finer *et al.*, 2018). Nevertheless, cloud cover constitutes a serious obstacle to EWS based exclusively on optical data in tropical forest environments. A recent survey among users pointed to cloud cover as the most important effectiveness limiting factor to the actual EWS (Weisse *et al.*, 2019). Hansen et al. (2016), reports 80% cloud cover during the wet season on Peru Landsat-7/8 data. In Brazil, frequent observations over Amazonian basin are seriously affected, as mean annual cloud cover on the Brazilian part of the biome is approximately 74%.
Orbital active microwave sensors, namely Synthetic Aperture Radar (SAR) satellites can help bridging this observational gap. SAR observations aren't blocked (though it can be affected) by atmospheric effects (Reiche *et al.*, 2016), and have greatly raised its availability after the launch of Sentinel-1A and B C-band SAR satellites. Some factors have limited the widespread adoption of SAR data in EWS. Among them we can cite:

1. Separability of classes: SAR researchers have struggled to distinguish different stages of forest succession, being the results normally inferior to the optical inferred classifications (Almeida-Filho *et al.*, 2005; Mercier *et al.*, 2019)
2. The ambiguity of the SAR signal change after a disturbance episode: although most of the time deforestation causes a drop on backscattering, some conditions can lead to an increase after a forest disturbance event (Almeida-Filho *et al.*, 2005; Shimabukuro *et al.*, 2007; Whittle *et al.*, 2012; Watanabe *et al.*, 2017).
3. Atmospheric factors affecting measurements: ionospheric and tropospheric effects can modify and even make unusable SAR data. Mitigation of these effects is somewhat complex and sometimes unfeasible (Kasilingam *et al.*, 1997; Davies and Smith, 2002; Marzano, Mori and Weinman, 2010).
4. Rain interception on the vegetation and soil moisture affect, sometimes intensely, backscattering values. The scarcity of rain gauges and moisture measurements makes mitigation of these effects challenging on operational contexts (De Jong, Klaassen, and Ballast, 2000; Cisneros Vaca and Van Der Tol, 2018; Benninga, 2019).

It is worth noting that, while atmospheric interference will normally attenuate C-band backscattering, rain interception may slightly increase SAR signal. Those effects can co-exist and even superpose over the same location.
More importantly, rain attenuation can mislead a potential automatic deforestation detection algorithm, thus increasing its false-positive rates.
This works aims to explore a comprehensive time-series SAR dataset to determine the potential relationship between backscattering and precipitation. For that purpose, Sentinel-1 SAR data were combined with hourly precipitation data coming from NASA's Integrated Multi-satellitE Retrievals for GPM (IMERG). Our objective was to determine the existence an optimal threshold able to mask most of the rain-related anomalies while preserving SAR information.

## 2. MATERIALS

### 2.1 Area of interest

The study sampled 993 locations in the Amazonia biome (Figure 1). The locations were randomly selected from the intact forest landscapes (IFL) 2016 dataset (Potapov *et al.*, 2017). Before


https://doi.org/10.5194/isprs-archives-XLII-3-W12-2020-493-2020 
Primary publication at IEEE Xplore: https://doi.org/10.1109/LAGIRS48042.2020.9165566

sampling, an internal buffer of 5 km was applied to the IFL polygons to avoid border effects.

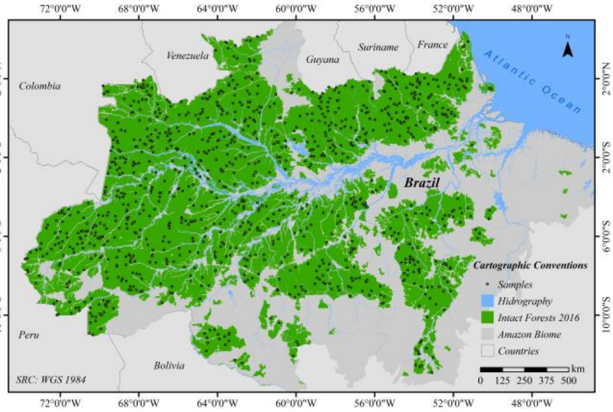


Figure 1: Map of sampled locations.

### 2.2 SAR data

For every sampled location, we collected Sentinel-1A/1B VH and VV backscattering values from 01/01/2017 to 01/01/2019 using Google Earth Engine platform (GEE, Gorelick et al. 2017). Pixel samples were denoised using a 7x7 Frost speckle filtering (Frost *et al.*, 1982) and converted to $\gamma^0$ values using local incidence angle, which should be enough to control backscattering variations on low-to-medium slope areas (Small, 2011). To maximize the homogeneity of the sampling locations, we excluded the locations where the mean backscatter value was outside the ($P_{10}$, $P_{90}$) percentile interval defined by the ensemble of locations backscattering means, for both polarities. This trimming reduced to 729 the number of forest locations considered for the study, which represents a total number of 52,611 backscattering observations through the entire two-years timespan and 9,044 different Sentinel-1 scenes. Table 1 summarizes the properties of the retained time-series.

| Polarization | Mean | Standard Deviation | Coefficient of Variation |
|---|---|---|---|
| VH | 0.057 | 0.0016 | 2.82 |
| VV | 0.231 | 0.0089 | 3.87 |

Table 1: Statistical values for sampled $\gamma^0$ time series.

### 2.3 Precipitation data

Along with backscattering, precipitation data were collected. The selected precipitation dataset was NASA's Integrated Multi-satellitE Retrievals for GPM (IMERG), on his version 06 (Huffman *et al.*, 2019). IMERG delivers global calibrated precipitation data on 0.1° (roughly 10x10 km) resolution, with a cadence of 30 minutes. For this study we computed the hourly mean calibrated precipitation rate (in mm/hr) for every backscattering sample, starting 12 hours before the time of SAR acquisition until 3 hours after. Other available precipitation datasets, such as CHIRPS (Funk *et al.*, 2015), weren't taken into account due to the insufficient temporal resolution.

## 3. METHODOLOGY AND RESULTS

### 3.1 Identification of SAR anomalies

To determine which SAR observations could be considered as being anomalous on a consistent way, we modeled the distribution of $\gamma^0_{VH}$ and $\gamma^0_{VV}$ values assuming them to follow a Gamma distribution (eq. 1).

$$f(x;\alpha,\beta) = \frac{\beta^{\alpha} x^{\alpha-1} e^{-\beta x}}{(\alpha-1)!} \tag{1}$$

Although all sampled locations are supposed to correspond to homogeneous forested areas, heterogeneities in the upper canopy structure can lead to variations on $\gamma^0$ values, especially in VV values (see Figure 2). To evaluate the effect of these heterogeneities, we adopted an modeling approach where a different Gamma distribution was fitted for every location backscattering time-series.

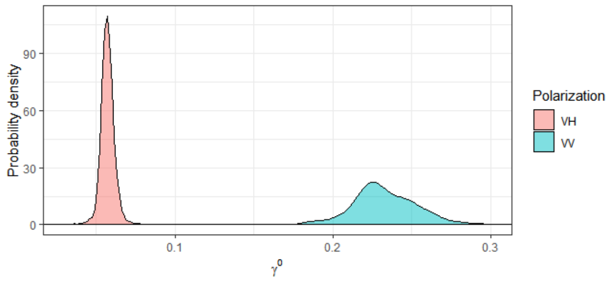


Figure 2: Mean $\gamma^0$ for sampled points density distribution.

Based on the obtained Gamma distribution parameters, and using a significance value of 1%, we defined the maximum and minimum thresholds which will define anomalous $\gamma^0$observations. 1% significance value was adopted to keep results consistent with authors' on-going research on deforestation detection.

| Polarization | Shape (α) | Rate (β) | $T_{min}$ | $T_{max}$ |
|---|---|---|---|---|
| VH | 191 | 3297 | 0.482 | 0.0681 |
| VV | 199 | 857 | 0.194 | 0.270 |

Table 2: Median parameters of the modelled gamma distribution parameters, and corresponding anomalies thresholds ($\alpha = 0.01$).

Based on the obtained thresholds, every backscattering observation was classified as normal observation, negative anomaly (when $\gamma^0 < T_{min}$) or positive anomaly (when $\gamma^0 > T_{max}$). Table 3 summarizes the number of observations flagged as anomalous.

| Pol. | Anomaly type | | Anomaly type (%) | |
|---|---|---|---|---|
| | Negative | Positive | Negative | Positive |
| VH | 455 | 486 | 0.86 | 0.92 |
| VV | 466 | 537 | 0.89 | 1.02 |

Table 3: Absolute and relative number of anomalous observations.

### 3.2 Analysis of backscattering response to precipitation

Using R package (R Core Team, 2013), we adjusted a set of generalized additive models (GAM) to the ensemble of $\gamma^0$ backscattering observations, using the accumulated rain as the independent variable. To get a detailed insight into the evolution of the backscattering as a function of the time of precipitation, we computed and plotted a model taking into account the accumulated rain for every hour interval before radar acquisition. Figure 3 shows the results of the GAM modeling for VH and VV polarizations. Additionally, we plotted and modeled the computed hourly precipitation rate versus backscattering values (Figure 4). These hourly charts will help establishing the potential time span of influence of rain over SAR acquisitions.

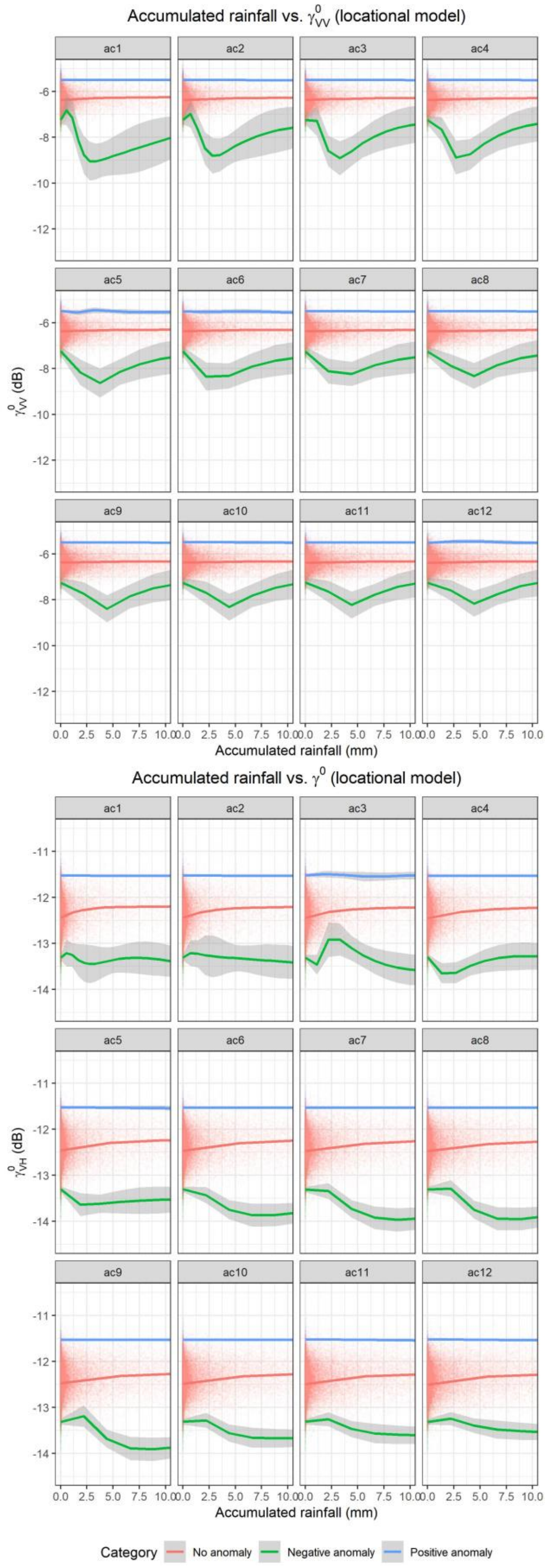


Figure 3: VV and VH $\gamma^0$ values vs. accumulated rainfall. Ac[i] refers to the accumulated rain [i] hours before the acquisition of the SAR data. Continuous lines are GAM models. Grey shades represent model 95% confidence interval.

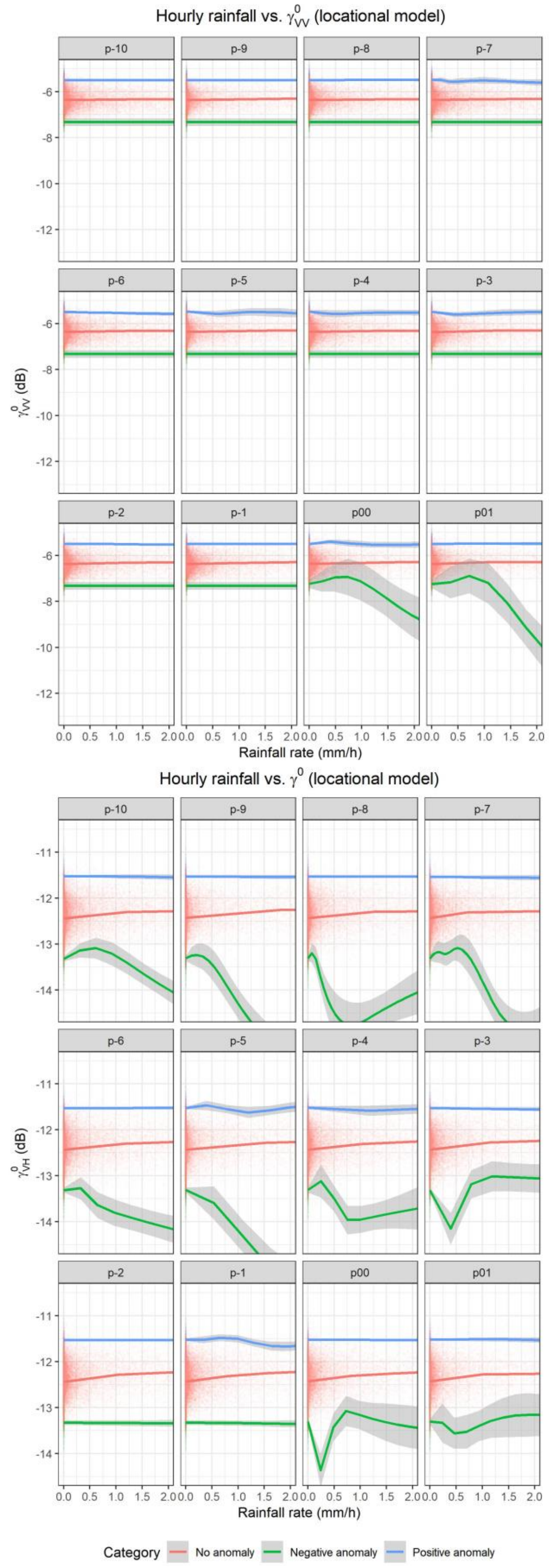


Figure 4: VV and VH $\gamma^0$ values vs. hourly rainfall rate. P-[i] refers to the rain rate [i] hours before the acquisition of the SAR data. p01 refers to rain one hour after. Continuous lines are GAM models. Grey shades represent model 95% confidence interval.

### 3.3 Backscattering masking as a function of accumulated and hourly precipitation

After checking the relationship between rainfall rate and backscattering values, we studied the feasibility of a rain-dependent masking strategy for radar data. This approach has been tested in soil moisture determination algorithms by Benninga, van der Velde, and Su (2019). In our case, by filtering backscattering observations based on rainfall we intend to reduce the number of anomalous values, and thus, to improve the results of a hypothetical deforestation detection algorithm.

To test this approach, we implemented an iterative algorithm that rejected all backscattering observations related to a specific rain quantity accumulated after a specific number of hours before the acquisition. After this filtering, we recount anomalies, to see if the number and proportion of negative and positives anomalies decreased, as we will expect.

The results of this screening procedure are shown in Figure 5 and Figure 6 in terms of % of anomalies and total observations reduction:

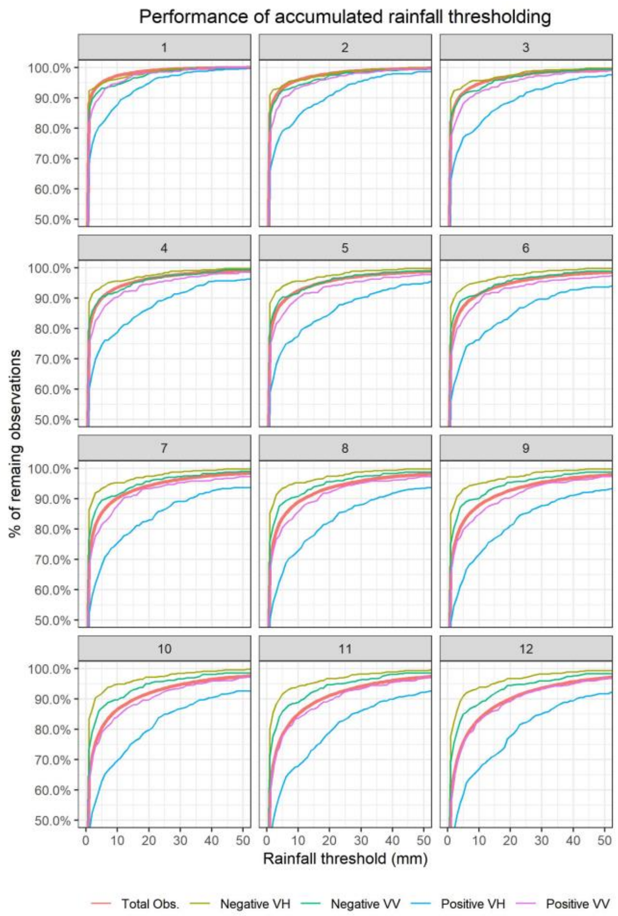


Figure 5: Results of SAR observation masking based on accumulated rain. Every chart corresponds to the number of hours before SAR acquisition that are being considered for precipitation summation. Thresholds are represented in the horizontal axis, while the vertical axis represents the percentage of total and anomalous observations that were preserved after masking.

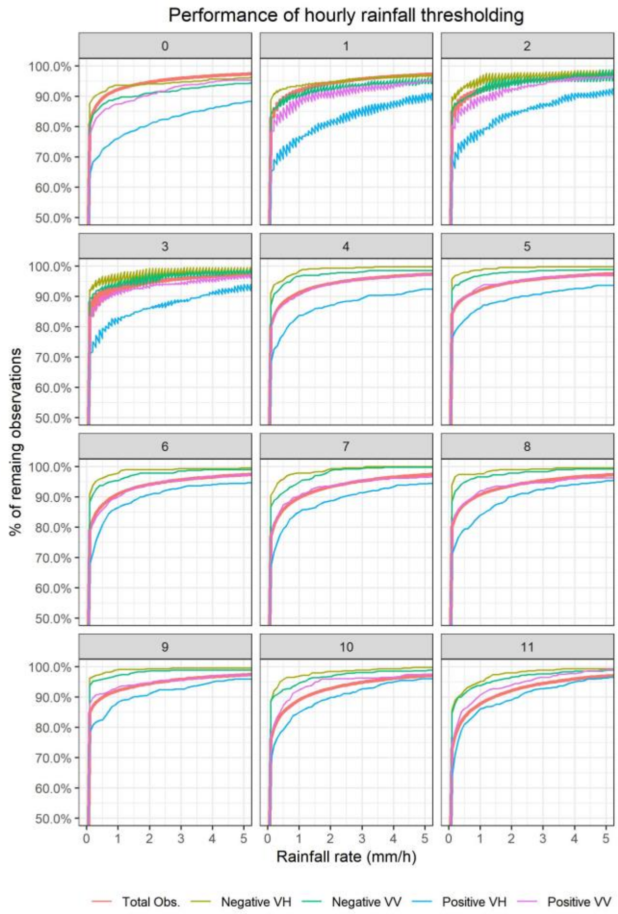


Figure 6: Results of SAR observation masking based on hourly rain rate. Every chart corresponds to the number of hours before SAR acquisition that are being considered for precipitation rate computation. Thresholds are represented in the horizontal axis, while the vertical axis represents the percentage of total and anomalous observations that were preserved after masking.

## 4. DISCUSSION

The charts and models plotted on figures 3 and 4 allows one to accomplish a thoughtful analysis of the relationship between rainfall and backscattering in a tropical environment. Regarding normal values, an increase in accumulated precipitation seem to slightly increase C-band SAR backscattering due to the temporary increase in the wetness of the upper canopy. This results is consistent with previous research (De Jong, Klaassen and Ballast, 2000; Benninga, van der Velde, and Su, 2019). We can quantify this increase in an approximate rate of 0,4 and 0,2 $dB/mm \cdot h^{-1}$, for VH and VV polarization respectively. As saturation levels are reached quickly (around 1 $mm \cdot h^{-1}$), total increase in backscattering due to precipitation will rarely reach 0,5 dB. Cisneros Vaca and Van Der Tol (2018) report higher anomalies (+1.5 dB on VH polarization) over temperate forests.

Regarding detected positive anomalies the models plotted on figures 3 and 4 don't show a significant correlation of $\gamma^0$ values with accumulated rain or with the rain rate during the acquisition or before it. That probably means that, although rain can raise backscattering by wetting canopy scatterers, this effect is not strong enough to raise backscattering measures above the 99% anomaly threshold. Hence, most of the detected positive anomalies should be provoked by other phenomena, such as uncontrolled speckle noise, man-made structures, or (most probably) terrain slope.

On the other side, $\gamma^0$ negative anomalies, which can become an important source of error on deforestation detection algorithms, seem to suffer a strong influence from rain patterns, as shown by figures 3 and 4 (green lines). This attenuation seems to impact VH backscattering when the instantaneous rain rate at the moment of the acquisition reach more than 1 mm/h (Figure 4, p00 and p01 panels). Strong decrease effects due to rain between 4 and 10 hours seem to be spurious (Figure 4, p-10 to p-3 panels), and should be investigated. VV data seem to suffer attenuation (much stronger than VH) starting at 0,8-1 mm/h.), which would peak around 5 mm of accumulated rain and then will saturate and decrease (Figure 3).

As exposed by Danklmayer et al. (2009), this substantial attenuation in backscattering is probably due to the strong absorption of electromagnetic energy as it passes through dense tropical rain cells. A recent example of that kind of phenomenon is shown in Figure 7, which depicts the impact of the passage of a super-storm cell on S1 $\gamma^0$ values. Point P1 registered a fall of 6 dB on both S1 polarizations on $5^{Th}$ August 2019 acquisition, which can be visualized as a purple stain on a multitemporal mosaic. An exceptionally thick storm cloud was registered by Sentinel-5p satellite the same day on P2, some 15 km eastward (yellow cell). The optical thickness of the storm was greater than the saturation value of the S5p sensor (250 m). IMEGR data examination indicates that probably the same storm cell passed above the $\gamma^0$ anomaly area exactly at the moment of S1 acquisition.

Regarding backscattering masking based on accumulated and hourly precipitation, the results, shown by figures 5 and 6, weren't completely satisfactory. Although some anomalies tend to decrease when applying rain thresholds based in accumulated hourly rain (figure 5), the total number of observations will decrease jointly. For instance, in we mask all observations associated with a 10-hour accumulated rain of more than 5mm, we will retain 80% of the total observations, 65% of VH negative anomalies, 80% of VV negative anomalies, 93% of VH positive anomalies and 87% of positive VV anomalies. Higher thresholds will decrease even more the number of non-masked observations. We consider this 20% decrease in the total number of observations excessive on the context of an EWS and won't worth the 7-35% reduction on observed anomalies.

The scale difference between the size of the atmospheric events that are supposed to be behind backscattering anomalies (kilometric, after Iwashita and Kobayashi, 2019) and the 10x10 km resolution precipitation data is a key factor on the lack of performance of the applied thresholding technique. Even if GPM hourly precipitation data might detect heavy-rain events, most of the S1 pixels inside an anomalous GPM cell wouldn't be affected by the event and thus will be incorrectly masked.

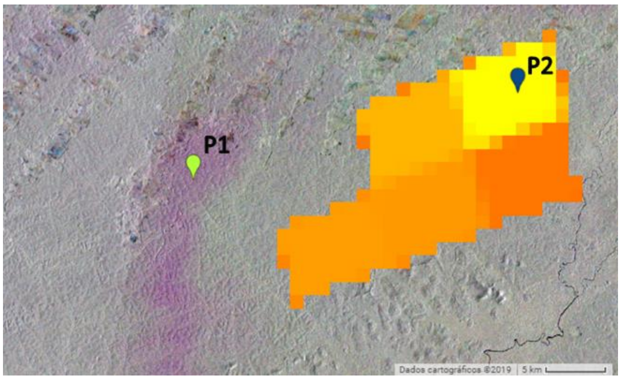


Figure 7: Sentinel-1 backscatter decay linked to super-storm cells in Roraima state (Brazil). The approximate size of the super-cell (in yellow) is 5x5 km.

## 5. CONCLUSIONS

In this study, we have considered a regional SAR and rainfall dataset to test the sensibility of SAR backscattering to short-term dense precipitation events. Our results confirmed that normal backscattering values suffer a minor increase (0,2-0,4 $dB/mm \cdot h^{-1}$) due to rain accumulated on the canopy on the hours before the SAR acquisition. In this case, Saturation levels are quickly reached. Abnormal high values (above percentile 99) are not significantly influenced by rain and may be mostly caused by other factors such as terrain slope. On the other hand, negative backscattering anomalies showed a strong relationship with rainfall, especially co-polarized (VV) backscattering values related to high rain rates recorded during the acquisition. This is probably due to dense rain-cell cloud attenuation.

Attempts to filter out backscattering anomalies by using precipitation-based thresholds weren't completely satisfying, as filtering masks out valid observations. This is probably due to the difference in the size of the rainfall data pixel and the size of the atmospheric events that provoke backscattering anomalies. Indeed, it has been verified that spatially coarse precipitation data provokes a great deal of incertitude in anomaly masking. Inside an IMEGR cell, a variety of atmospheric situations can happen simultaneously. More accurate results will need higher spatial resolution, such as that given by meteorological radars. A good example of the advantages of this kind of data can be found in Atlas, Rosenfeld, and Wolff (1993). Even if the results of our study should be considered with precaution, they constitute an operational guideline for deforestation detection algorithms optimization, taking in account that accurate screening of attenuation-affected backscattering observations will require higher resolution (at least 2x2 km) cloud density and/or rain rate information, with at least hourly resolution.

## ACKNOWLEDGMENTS

This study was financed in part by the Coordenação de Aperfeiçoamento de Pessoal de Nível Superior - Brasil (CAPES) - Finance Code 001

## REFERENCES

Almeida-Filho, R. et al. (2005) 'Evaluation and perspectives of using multitemporal L-band SAR data to monitor deforestation in the Brazilian Amazônia', IEEE Geoscience and Remote Sensing Letters, 2(4), pp. 409–412. doi: 10.1109/LGRS.2005.856679.

Assunção, J., Gandour, C. and Rocha, R. (2013) 'DETERring Deforestation in the Brazilian Amazon: Environmental Monitoring and Law Enforcement TL - May', Climate Policy Initiative Report, (May), pp. 1–36.

Atlas, D., Rosenfeld, D. and Wolff, D. B. (1993) 'C-band attenuation by tropical rainfall in Darwin, Australia, using climatologically tuned Ze-R relations', Journal of Applied Meteorology, 32(2), pp. 426–430. doi: 10.1175/1520-0450(1993)032<0426:CBABTR>2.0.CO;2.

Benninga, H.-J. F., van der Velde, R. and Su, Z. (2019) 'Impacts of Radiometric Uncertainty and Weather-Related Surface Conditions on Soil Moisture Retrievals with Sentinel-1', Remote Sensing, 11(17), p. 2025. doi: 10.3390/rs11172025.

Cisneros Vaca, C. and Van Der Tol, C. (2018) 'Sensitivity of sentinel-1 to rain stored in temperate forest', in International Geoscience and Remote Sensing Symposium (IGARSS). Valencia, Spain: IGARSS, pp. 5330–5333. doi: 10.1109/IGARSS.2018.8517859.

Danklmayer, A. et al. (2009) 'Assessment of atmospheric propagation effects in SAR images', IEEE Transactions on Geoscience and Remote Sensing, 47(10), pp. 3507–3518. doi: 10.1109/TGRS.2009.2022271.

Davies, K. and Smith, E. K. (2002) 'Ionospheric effects on satellite land mobile systems', IEEE Antennas and Propagation Magazine, 44(6), pp. 24–31. doi: 10.1109/MAP.2002.1167260.

De Jong, J., Klaassen, W. and Ballast, A. (2000) 'Rain storage in forests detected with ERS tandem mission SAR', Remote Sensing of Environment, 72(2), pp. 170–180. doi: 10.1016/S0034-4257(99)00100-5.

Finer, B. M. et al. (2018) 'Combating deforestation: From satellite to intervention', Science, 360(6395), pp. 1303–1305. doi: 10.1126/science.aat1203.

Frost, V. S. et al. (1982) 'A Model for Radar Images and Its Application to Adaptive Digital Filtering of Multiplicative Noise', IEEE Transactions on Pattern Analysis and Machine Intelligence, PAMI-4(2), pp. 157–166. doi: 10.1109/TPAMI.1982.4767223.

Funk, C. et al. (2015) 'The climate hazards infrared precipitation with stations - A new environmental record for monitoring extremes', Scientific Data, 2, pp. 1–21. doi: 10.1038/sdata.2015.66.

Gorelick, N. et al. (2017) 'Google Earth Engine: Planetary-scale geospatial analysis for everyone', Remote Sensing of Environment. The Author(s), 202, pp. 18–27. doi: 10.1016/j.rse.2017.06.031.

Hansen, M. C. et al. (2016) 'Humid tropical forest disturbance alerts using Landsat data', Environmental Research Letters. IOP Publishing, 11(3), p. 034008. doi: 10.1088/1748-9326/11/3/034008.

Huffman, G. J. et al. (2019) 'GPM IMERG Final Precipitation L3 Half Hourly 0.1 degree x 0.1 degree V06 (GPM_3IMERGHH) at GES DISC'. Greenbelt, MD: Goddard Earth Sciences Data and Information Services Center. doi: 10.5067/GPM/IMERG/3B-MONTH/06.

Iwashita, H. and Kobayashi, F. (2019) 'Transition of meteorological variables while downburst occurrence by a high density ground surface observation network', Journal of Wind Engineering and Industrial Aerodynamics. Elsevier Ltd, 184(June 2018), pp. 153–161. doi: 10.1016/j.jweia.2018.10.007.

Kasilingam, D. et al. (1997) 'Investigation of tropical rain cells with ERS SAR imagery and ground-based weather radar', in Third ERS symposium on space at the service of our Environment, Vols. Ii & Iii. (ESA Special Publications), pp. 1603–1608.

Marzano, F. S., Mori, S. and Weinman, J. A. (2010) 'Evidence of rainfall signatures on X-band synthetic aperture radar imagery over land', IEEE Transactions on Geoscience and Remote Sensing. IEEE, 48(2), pp. 950–964. doi: 10.1109/TGRS.2009.2034843.

Mercier, A. et al. (2019) 'Evaluation of Sentinel-1 and 2 Time Series for Land Cover Classification of Forest–Agriculture Mosaics in Temperate and Tropical Landscapes', Remote Sensing, 11(8). doi: 10.3390/rs11080979.

Nepstad, D. et al. (2014) 'Slowing Amazon deforestation through public policy and interventions in beef and soy supply chains', Science, 344(6188), pp. 1118–1123. doi: 10.1126/science.1248525.

Petersen, R., Renschler, K. and Weisse, M. (2018) Early Warning Systems for Deforestation: An explainer. Available at: https://blog.globalforestwatch.org/data-and-research/early-warning-systems-for-deforestation-an-explainer.

Potapov, P. et al. (2017) 'The last frontiers of wilderness: Tracking loss of intact forest landscapes from 2000 to 2013', Science Advances, 3(1), pp. 1–14. doi: 10.1126/sciadv.1600821.

R Core Team (2019) 'R: A Language and Environment for Statistical Computing'. Vienna, Austria. Available at: https://www.r-project.org/.

Reiche, J. et al. (2016) 'Combining satellite data for better tropical forest monitoring', Nature Climate Change. Nature Publishing Group, 6(2), pp. 120–122. doi: 10.1038/nclimate2919.

Shimabukuro, Y. E. et al. (2007) 'Quantifying optical and SAR image relationships for tropical landscape features in the Amazônia', International Journal of Remote Sensing, 28(17), pp. 3831–3840. doi: 10.1080/01431160701236829.

Small, D. (2011) 'Flattening gamma: Radiometric terrain correction for SAR imagery', IEEE Transactions on Geoscience and Remote Sensing, 49(8), pp. 3081–3093. doi: 10.1109/TGRS.2011.2120616.

Soares-Filho, B. et al. (2010) 'Role of Brazilian Amazon protected areas in climate change mitigation', Proceedings of the National Academy of Sciences, 107(24), pp. 10821–10826. doi: 10.1073/pnas.0913048107.

Watanabe, M. et al. (2017) 'Development of early-stage deforestation detection algorithm (advanced) with PALSAR-2/ScanSAR for JICA-JAXA program (JJ-FAST)', International Geoscience and Remote Sensing Symposium (IGARSS), 2017-July(July), pp. 2446–2449. doi: 10.1109/IGARSS.2017.8127487.

Weisse, M. J. et al. (2019) Use of near-real-time deforestation alerts: a case study from Peru. Washington, DC. Available at: https://www.wri.org/publication/use-near-real-time-deforestation-alerts.

Whittle, M. et al. (2012) 'Detection of tropical deforestation using ALOS-PALSAR: A Sumatran case study', Remote Sensing of Environment. Elsevier Inc., 124, pp. 83–98. doi: 10.1016/j.rse.2012.04.027.